YTUP

Journal of Thermal Engineering
https://jten.yildiz.edu.tr/
https://doi.org/10.47481/jten.0002

RESEARCH ARTICLE

Passive control techniques for mixing enhancement of mach 1.86 supersonic jet: a computational study

Bholu Kumar[1,*], Shantanu Srivastava[2], Devendra Kumar Lohia[3], Digamber Singh[4]

[1]Department of Mechanical Engineering, Poornima University, Jaipur Plot No. IS-2027-2031, Ramchandrapura P.O. Vidhani, Vatika Rd, Sitapura, Jaipur, Rajasthan, 303905, India
[2]Department of Mechanical Engineering, Motilal Nehru National Institute of Technology Allahabad, Prayagraj, 211004, India
[3]Department of Mechanical Engineering, Rama University, Rama City, Mandhana, Kanpur, Uttar Pradesh, 209217, India
[4]Department of Mechanical Engineering, Alliance University, Chikkahagade Cross, Chandapura - Anekal Main Road, Anekal, Bengaluru, Karnataka, 562106, India

Abstract

The present study aims to simulate both controlled and uncontrolled Mach 1.86 jets from a convergent–divergent nozzle using computational fluid dynamics (CFD). A rectangular cross-wire with a 5% area-blockage was used as a passive control device at the nozzle exit to enhance jet mixing. The two-dimensional nozzle model was created in ANSYS Workbench, and the governing equations were solved using the FLUENT solver with the realizable k–ε turbulence model. Simulations were performed for nozzle pressure ratios (NPR) ranging from 4 to 9. The results show that the jet core length decreases under controlled conditions, confirming enhanced mixing. Pressure variation significantly affected flow development: at moderate NPRs (5–6), the jet was overexpanded and showed a 21–27% core reduction, whereas at a higher NPR (9), stronger under expansion led to about a 37% reduction due to greater shear-layer instability and more intense vortex formation. Mach number contours are used to examine the presence of shocks in the jet and the wave structure. This study demonstrates the substantial benefits that a simple cross-wire used as a passive device offers in enhancing mixing in supersonic jets. The outputs of this study will be beneficial in suppressing aerodynamic noise, improving jet combustion, and enhancing propulsion efficiency.

Keywords: CFD, crosswire, jet mixing, passive control, supersonic

Cite this article as: Kumar, B., Srivastava, S., Lohia, D. K., & Singh, D. (2026). Passive control techniques for mixing enhancement of Mach 1.86 supersonic jet: A computational study. Journal of Thermal Engineering, 12(3), 2–13. https://doi.org/10.47481/jten.0002

1. Introduction

It is well established that the mean flow characteristics of a supersonic free jet can be predicted by both the transition SST turbulence model and the realizable k-ε model. However, most of the studies conducted so far are limited to the simulation of uncontrolled free jets. Limited work is being carried out on the computational simulation of the supersonic jet. Previous research efforts have provided an in-depth understanding of, including their fundamental flow aspects, flow mixing, and control schemes. Taken together, these works show that shock-cell structures, shear-layer instabilities, and nozzle geometry are key factors defining the spreading and entrainment of the jet. Experimental and computational studies have shown that passive devices, such as tabs, chevrons, and cross-wires, can greatly modify the jet shear layer and enhance mixing, whereas active techniques, though effective, often involve greater complexity and energy input. Moreover, prior CFD research supports the capability of RANS models to represent global jet dynamics, while highlighting the challenges in modeling unsteady structures in detail. However, systematic investigations of simple, cost-effective passive devices across various nozzle pressure ratios remain scarce, which justifies the present investigation.

Jet mixing in supersonic flows has important applications in aerospace propulsion, combustion systems, and jet noise suppression. The use of passive control elements such as tabs, chevrons, and cross-wires has been reported to affect the development of the shear layer and increase entrainment [1-2].

*Corresponding Author
E-mail Adress: bholu.kumar@poornima.ed.in

Submitted: 21 October 2025; **Accepted:** 17 November 2025

This paper was recommended for publication in revised form by Editorin-Chief Ahmet Selim Dalkılıç

These techniques alter flows by generating streamwise vortices that promote turbulent mixing without expending additional energy. On the contrary, active techniques such as acoustic excitation and fluidic injection-while effective-are not energy efficient as they require additional power and complex mechanisms [3]. This has made the development of compact and energy-efficient designs unfeasible. The research of Zaman [1], for example, focused on the use tabs and high Mach numbers, while Panda and Seasholtz [4] studied high nozzle pressure ratios (NPRs) and reported the presence of strong shock-vortex interactions, which aided in enhanced mixing. Overall, the research suggests that the effectiveness of passive devices to control jet mixing relies heavily on both flow compressibility and NPR.

The controlled jet was first studied experimentally by Bradbury and Khadem [5]. The jet cross section was found to be considerably distorted by the tabs and to be instrumental in enhancing the jet spread. Although the study was confined to the subsonic jets, it nevertheless shed some light on the development of controlled jets. The mixing enhancement of the jet regulated by tabs at the nozzle exit was studied by Zaman et al. [6,7] and Ahuja et al. [8]. According to them, the tabs improve jet mixing across all Reynolds numbers. These flow characteristics are typical of a supersonic jet. The investigation of the jet mixing, with different tab configurations by placing 2, 4, 6 and 8 tabs at the nozzle exit, was done by Zaman et al. [9]. It was found that just two tabs positioned opposite one another are sufficient to cause gross jet distortion and enhance jet mixing. Previous work also highlighted that, in order to ensure efficient jet mixing, the tab height needs to be larger than the boundary layer thickness near the jet exit [10]. Nevertheless, N.K. Singh and Radhakrishnan [11] demonstrated that, the tab height should be kept maximum up to the jet centreline, for an axisymmetric jet. Two tabs, positioned across from one another along the diameter, significantly enhance jet mixing. Tabs that, when placed diametrically opposite each other and able to meet at the jet centreline, are called limiting tabs. The limiting tab could be thought of as a cross-wire that can have any defined cross-section, such as circular or rectangular. The effect of limiting tab on the supersonic jet mixing for convergent-divergent square-cross section nozzle, was studied experimentally by Shantanu and Radhakrishnan [12], Shantanu and Kaushik [13]. It was discovered that adding a cross-wire at the nozzle exit allowed a significant reduction in core length. The effectiveness of the "air tab" method, which involves jet mixing via air injection at a determined angle of attack, is being investigated by Balaji et al. [14]. Manikandan et al. [15] further documented that smaller air tabs promote jet mixing more effectively by shortening the core length and increasing the rate of velocity decay. Optimally, balanced air mixing control and maximum mixing efficiency are achieved with the optimal tab size. The combination of the injection strategy and vortex generators leads to a large increase in aerodynamic performance: lift increases by 42% and drag decreases by 44%. This novel approach is promising in enhancing the efficiency of aircraft wings [16]. For supersonic engine testing, nozzle choking is vital to provide a constant mass flow rate at specified operating temperature and pressure. Moreover, for performance evaluation of the engine, the choked nozzle is necessary to maintain flow stability [17]. Akhil et al. [18] proved that different strut configurations and fuel injection positioning in a scramjet combustor resulted in combustion efficiency improvements to 99% with a slight pressure loss. This enhanced design is a breakthrough for supersonic propulsion, achieving Mach 2 with superior performance and efficiency. Augmenting the work of Manikanta et al. [19], wall length serves as a vital jet behavior modification parameter with wide thrust vectoring and advanced jet performance for high-speed aircraft configurations. Consequently, Illyas et al. [20] compared different configurations of an impinging jet and concluded that slotted jets generate more radial velocity and crosswise heat transfer than circular jets, overcoming the highly turbulent regions of the jets and high Nusselt number gradient zones with lower jet to plate spacing. Thakare [21] studied the performance of vortex tubes in relation to the cold mass fraction and exergetic efficiency, revealing maximums of 27.77% and 39.39% cold and hot at 600kPa, respectively.

Launder and Spalding [22] demonstrated that the k-epsilon turbulence model is potentially effective in predicting near-wall and free shear flow phenomena. However, the researchers admitted that the applications are limited to low-Reynolds-number flows and that the near-wall region requires treatment to account for Mach-number effects on the length scales. Dash et. al. [23], fully explained the k-ε CDJ model, which is an expanded form of the k-ε turbulence model. This model incorporates the effects of vortex stretching and compressible dissipation to enable precise simulation of supersonic jets. However, it was revealed that, for the supersonic jets, the vortex-stretching correction posed problems on the jet axis at the location of shock impingement. Thus, it was envisaged that the basic Reynolds-stress substitution could more accurate in predicting the flow parameters of the supersonic jet. Tam and Thies [24] demonstrated that, the jet mean flow predictions can be made precisely by selecting new set of empirical constants for the k-ε turbulence model. It was also emphasized that the initial conditions required for accurate predictions of cold jets are easier to construct than those for hot jets. Evgenevna et. al. [25] explored differential turbulence models with two parameters to compute supersonic gas jets. The transition SST and realizable k-ε turbulence models could be applied to accurately predict the flow parameters.

Building on these observations, the present work focuses on simulating uncontrolled and controlled jets. The jet considered here is controlled by a rectangular cross-wire at the nozzle exit. The results are illustrated by a graph of total pressure as a function of axial distance, which is also known as centerline pressure decay (CPD). The extent of jet mixing is determined by the core lengths of both controlled and uncontrolled jets. In addition, the qualitative analysis of the jet includes the shock-cell structure and the primary waves in the jet field, which are visualized using Mach number contours.

2. Methodology for simulation

To lower the computational cost of CFD simulations for uncontrolled jets, a simplified axisymmetric model is developed for numerical investigation. However, the full domain was constructed for computational investigations of the controlled jet to visualize the effect of the cross-wire positioned at the nozzle exit. These computational domains extend to about 30 times the nozzle-exit diameter (30D, with D being the nozzle-exit diameter) along the jet axis from the nozzle outlet and to approximately 10D normal to the jet axis. Computational grids are generated using the ANSYS ICEM module, and the analysis is performed using the FLUENT solver. Figure 1 provides a detailed description of all steps involved in completing the computational work.

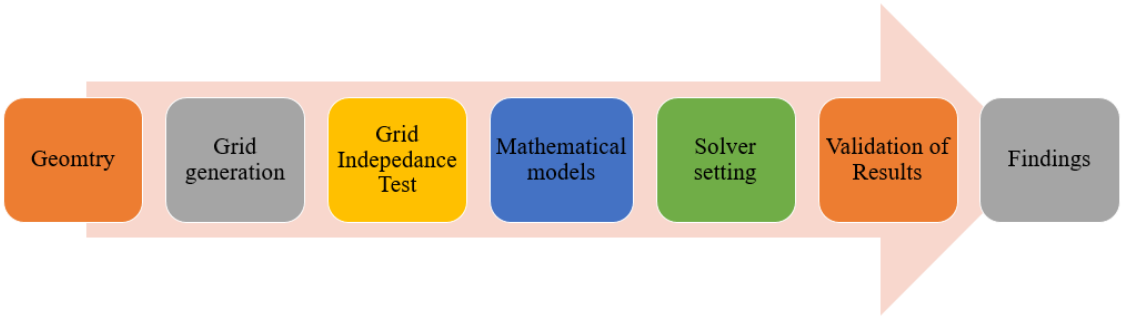

Figure 1. Glimpse of computation work

2.1. Numerical domain

A two-dimensional CFD model was used in this work. The primary justification is its ability to substantially reduce computational time and resource requirements while still capturing the dominant flow characteristics. Previous studies [26-28] have shown that 2-D models can provide sufficiently accurate predictions for preliminary investigations of similar flows.

The standard values for the convergent section and the divergent section of the nozzle is 15^0 degrees and 7^0 degrees, accordingly. In order to avoid flow separation, the flow expansion at the nozzle exit is restricted to a maximum divergence angle of 7^0 degrees. The Area-Mach relation that available in the several book of compressible flow/gas dynamics has been utilised to design the Mach 1.86 jet for the present investigation [29-30]. Figure. 2 presents the CAD model of the nozzle and the computational domain.

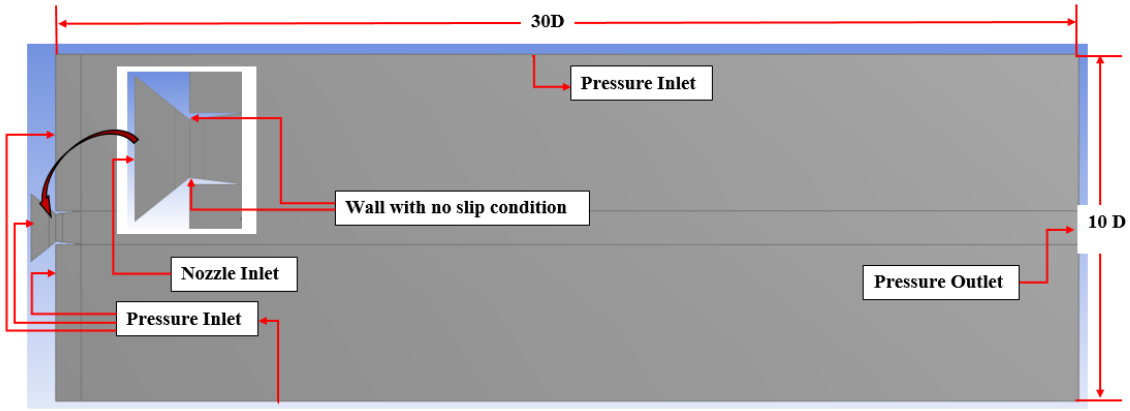

Figure 2. CAD model of convergent-divergent nozzle with computational flow domain

2.2. Meshing

The meshing module of ANSYS Workbench is used to generate 2-dimensional quadrilateral grids for both uncontrolled and controlled jets. For the 2-D quadrilateral structured grids, grid sizes of 5.6E+4, 8.7E+4, 11.4E+4, 12.6E+4, 15.4E+4, 22.3E+4, and 34.9E+4 are generated, as illustrated in Figure 3. The schematic diagram of the nozzle, including the flow domain that defines its boundaries, is presented in Figure 4.

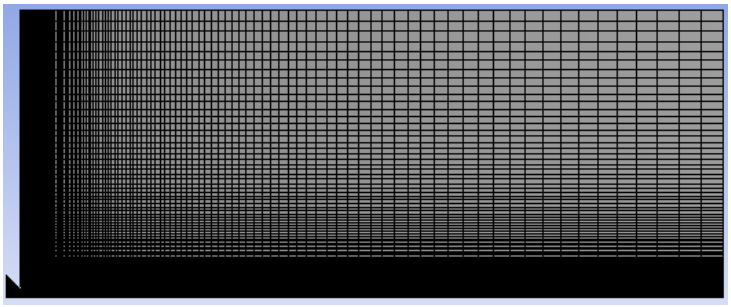

Figure 3. Computational grid for uncontrolled jet

The predetermined axial locations used for the grid-independence test across different grid sizes are shown in Figure 5. The grid at which the computational result is no longer dependent on grid size is identified by computing the Mach number at various grid sizes. The results show that grid sizes greater than 22.3E+4 have no significant effect; therefore, a grid size of 22.3E+4 was used for the present study. The maximum skewness (0.43) and aspect ratio (2.38) are obtained for the adopted grid size of 22.3E+4.

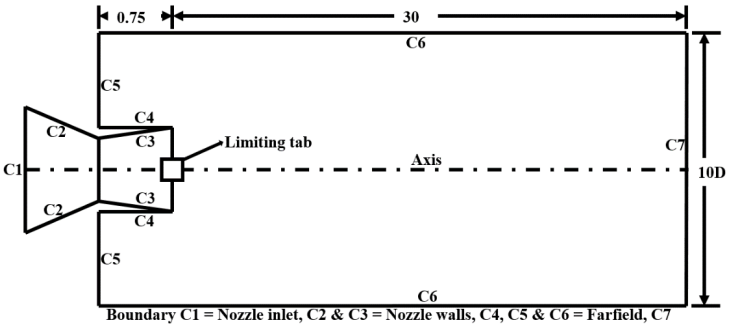

Figure 4. Diagrammatic representation of the computational domain

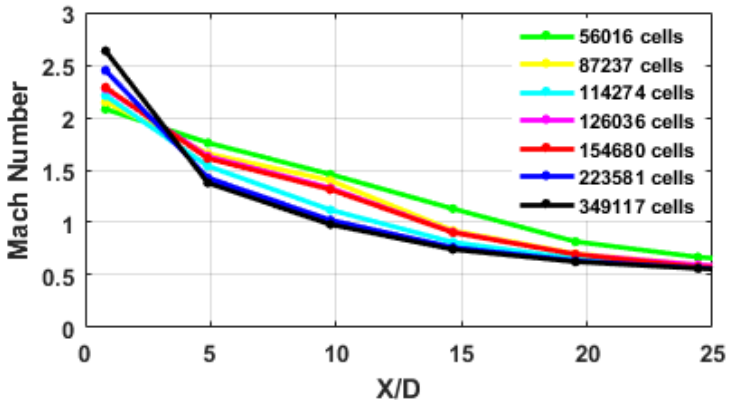

Figure 5. Grid Independence test for uncontrolled jet

The grids are evenly refined along the jet axis and in the near-field region. There is no shear layer at the edge of the domain; therefore, coarse grids in this region can be used without loss of accuracy. Strong gradients of scalar fields are generated by large-scale vortices formed in the free shear layer that develops between the surrounding fluid and the jet at the nozzle exit. These vortices entrain the jet field. Therefore, a fine mesh is needed only inside the nozzle and along the jet axis.

Structured quadrilateral grids for the controlled jet are generated using the same approach applied earlier to the uncontrolled jet, as shown in Figure 6. With reference to the grid-independent mesh size of the above uncontrolled jet, the grid size of the controlled jet is generated in the same proportion for the full-domain study. Hence, the grid independence test was conducted for the grid sizes 18.4E+3, 32.8E+3, and 63.6E+3, as presented in Figure. 7. The simulation results beyond 32.8 E+3 do not change between computations using different grid sizes. Hence, a grid size of 32.8E+3 is adopted for the controlled-jet simulation in the present study. A maximum aspect ratio of 5.98 and a skewness of 0.43 are reported for this 32.8E+3 grid size.

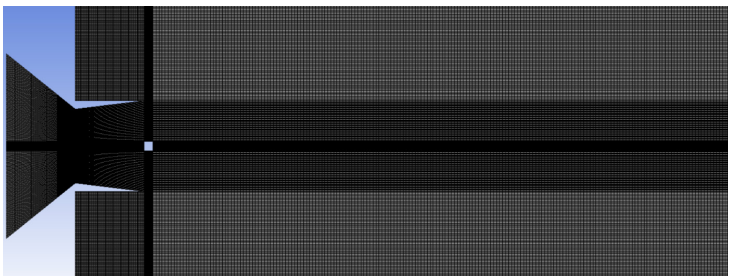

Figure 6. Grid for controlled jet computation (enlarged view)

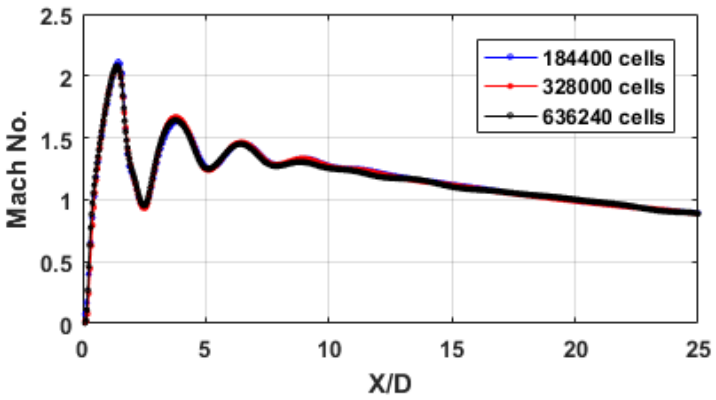

Figure 7. Mesh Independence assessment for controlled jet

The mesh-quality matrix for both uncontrolled and controlled jets, at the selected grid size and relative to the GIT result, is shown in Table 1.

Table 1. Mesh quality matrix of uncontrolled and controlled jets.

Mesh Property	Uncontrolled Jet	Controlled Jet
Element size	223581	328000
Maximum Aspect ratio	1.98	5.98
Maximum Skewness	0.43	0.43
Average Orthogonal quality	0.99	0.99
Average Element quality	0.99	0.72

3. Numerical procedures

The governing PDEs constitute the Navier-Stokes system, which is solved using finite-volume methods in the FLUENT solver. The equations are solved using double-precision accuracy. The flow, kinetic energy, and other associated convective variables are described by the second-order upwind technique.

3.1. Governing equations

The governing equation employs the Navier-Stokes system in its conservative form. The Navier-Stokes system of equations consists of the conservation laws for mass, momentum, and energy, which are represented mathematically by partial differential equations. The equations are given below.

$$\frac{\partial \rho}{\partial \tau} + \nabla \cdot \left(\rho \vec{V}\right) = 0 \quad (1)$$

$$\frac{\partial (\rho u)}{\partial t} + \nabla \cdot \left(\rho u \vec{V}\right) = -\frac{\partial p}{\partial x} + \frac{\partial \tau_{xx}}{\partial x} + \frac{\partial \tau_{yx}}{\partial y} + \rho f_x \quad (2)$$

$$\frac{\partial (\rho v)}{\partial t} + \nabla \cdot \left(\rho v \vec{V}\right) = -\frac{\partial p}{\partial y} + \frac{\partial \tau_{xy}}{\partial x} + \frac{\partial \tau_{yy}}{\partial y} + \rho f_y \quad (3)$$

$$\frac{\partial}{\partial t}\left[\rho\left(e + \frac{V^2}{2}\right)\right] + \nabla \cdot \left[\rho\left(e + \frac{V^2}{2}\vec{V}\right)\right] = \rho q + \frac{\partial}{\partial x}\left(k\frac{\partial T}{\partial x}\right) + \frac{\partial}{\partial y}\left(k\frac{\partial T}{\partial y}\right) - \frac{\partial (up)}{\partial x} + \frac{\partial (u\tau_{xx})}{\partial x} + \frac{\partial (u\tau_{yx})}{\partial y} + \frac{\partial (v\tau_{xy})}{\partial x} + \frac{\partial (v\tau_{yy})}{\partial y} + \rho \vec{f}\vec{V} \quad (4)$$

The above equations represent the conservation of mass (equation 1), momentum along the x-axis (equation 2), momentum along the y-axis (equation 3), and energy (equation 4).

3.2. Turbulence model

To evaluate the mixing performance of controlled and uncontrolled jets and to quantify turbulence characteristics, the most widely used realizable k-epsilon turbulence model was employed.

The realizable k-epsilon turbulence model was chosen for these simulations because it strikes an optimal balance between computational expense and predictive capability for free-shear and jet-like mixing layers in high-Reynolds-number turbulence. The realizable formulation, compared with the standard k-epsilon model, improves the prediction of the mean strain and swirl and relaxes enforcement of physical bounds on the Reynolds stresses; within a Reynolds-averaged approach, this relaxation helps capture the decay and spread of a supersonic free jet. For the current 2D parametric study that varies the nozzle pressure ratios and passive control configurations, the realizable formulation of the k-epsilon model allows efficient computation of multiple cases and flow fields whose integral quantities (centerline pressure decay, jet core length, and pressure distributions) provide reasonable agreement with the benchmark data.

The transport equations are used exactly as written to determine the turbulent kinetic energy and dissipation [31].

$$\frac{\partial}{\partial t}(\rho k) + \frac{\partial}{\partial x_j}(\rho k u_j) = \frac{\partial}{\partial x_j}\left[\left(\mu + \frac{\mu_t}{\sigma_k}\right)\right] + P_k + P_b - \rho\epsilon - Y_m + S_k \quad (5)$$

$$\frac{\partial}{\partial t}(\rho \epsilon) + \frac{\partial}{\partial x_j}(\rho \epsilon u_j) = \frac{\partial}{\partial x_j}\left[\left(\mu + \frac{\mu_t}{\sigma_\epsilon}\right)\frac{\partial \epsilon}{\partial x_j}\right] + \rho C_1 S_\epsilon - \rho C_2 \frac{\epsilon^2}{k + \sqrt{\vartheta}} + C_{1\epsilon}\frac{\epsilon}{k}C_{3\epsilon}P_b + S_\epsilon \quad (6)$$

Here, μ and μ_t denote the coefficients of dynamic and eddy viscosity, respectively, and the turbulent Prandtl numbers for k and ϵ are denoted by σ_k and σ_ϵ, respectively. Generations of turbulent kinetic energy P_k is due to the mean velocity gradient and P_b to buoyancy. Y_m represents the variable dilatation contribution to the total dissipation rate in compressible turbulence. The terms "S_k" and "S_ϵ" are user-defined source terms. It is now possible to evaluate the model constant, C_1 as

$$C_1 = \max\left[0.43, \frac{\eta}{\eta+5}\right],\ \eta = S\frac{k}{\in},\ S = \sqrt{2}\,S_{ij} \quad (7)$$

Where the strain tensor is represented by S_{ij}, while the mean strain rate is denoted by S. The model for turbulent viscosity is

$$\mu_t = \rho C_\mu \frac{k^2}{\in} \quad (8)$$

Where,

$$C_\mu = \frac{1}{A_0 + A_s\frac{KU^*}{\in}}$$

$$U^* = \sqrt{S_{ij}S_{ij} + \tilde{\Omega}_{ij}\tilde{\Omega}_{ij}}$$

$$\tilde{\Omega}_{ij} = \Omega_{ij} - 2\epsilon_{ijk}\omega_k$$

$$\Omega_{ij} = \dot{\Omega}_{ij} - \epsilon_{ijk}\omega_k$$

The variable " Ω_{ij} " represents the average rate-of-rotation tensor, as perceived in an angular velocity-rotating reference frame. Given by the model constants and

$$A_0 = 4.04$$

$$A_s = \sqrt{6}\cos\varnothing$$

$$\varnothing = \frac{1}{3}\cos^{-1}(\sqrt{6}\,W)$$

$$W = \frac{S_{ij}S_{jk}S_{ki}}{\tilde{S}^3},\ \tilde{S} = \sqrt{S_{ij}},\ S_{ij} = \frac{1}{2}\left(\frac{\partial u_j}{\partial x_i} + \frac{\partial u_i}{\partial x_j}\right)$$

$$C_{1\epsilon} = 1.44, C_2 = 1.9, \sigma_k = 1.0, \sigma_\epsilon = 1.2$$

3.2.1. Turbulence Model Selection and Comparison

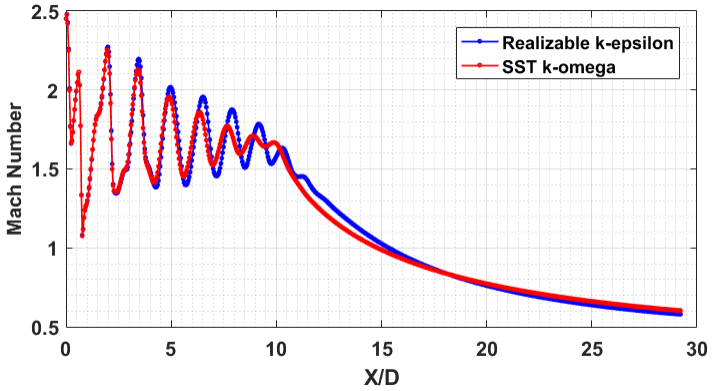

Figure 8. Comparison of turbulence model

A comparative study was conducted to validate the efficacy of the realizable k–ε and SST k–ω turbulence models in simulating supersonic jet mixing. Considering its moderate computational cost, the realizable k-ε model matched centreline pressure decay and jet-spreading benchmark data more closely than any other model. The SST k-ω model, while providing higher accuracy in the near-wall regions, exhibited greater numerical diffusion in the jet shear layer, which affected the accuracy of jet core length prediction. Standard k-ε and RNG k-ε models were omitted from the comparison because previous studies demonstrated their inability to simulate compressible, high-speed free jets with strong shock-vortex interactions. These models neither predict the jet spreading rate satisfactorily nor capture shear-layer instabilities. Thus, the only models analysed were the realizable k-ε and SST k-ω models, since these are the most commonly used and validated for high-Reynolds-number compressible jet applications.

3.3. Boundary conditions

The boundary conditions represented by the letters C1, C2, C3, C4, C5, C6, and C7 are shown in Figure 4. For NPRs between 4 and 9, the pressure inlet boundary condition is applied at boundary C1. At boundary C1, the temperature is kept consistently at 300 K. The wall boundary condition is applied for the walls of the nozzles identified as C2 and C3, and it is assumed that both of them are adiabatic and adhere to the no-slip condition. The nozzle walls, including the cross-wire, are modelled using normal wall functions. Boundary C7 is assigned a pressure-outlet boundary condition; pressure-inlet boundary conditions are applied at C4, C5, and C6. For simulations of the uncontrolled jet, using an axisymmetric domain is the most computationally efficient approach. Figure 4 shows that, in this case, an axis boundary condition is applied along the jet axis, which explains why the condition is satisfied. The boundary conditions above are summarised in the table below.

Table 2. Boundary conditions

Boundary	Applied boundary condition	Remark
Nozzle Inlet	Pressure Inlet Boundary condition	Boundary C1, NPR variation : 4 to 9
Nozzle Wall	Wall boundary condition with no slip	Boundary C2 and C3
Farfiled	Pressure inlet	Boundary C4, C5 and C6
Outlet	Pressure outlet	Gauge pressure = 0 Pa
Solver type	Density Based	Density Based
Operating Pressure	101325 Pa	Temperature = 300K

3.4. Simulation setup

As mentioned, the computational study accounts for the conservation of mass, momentum, and energy, as well as for the transport equations of turbulent kinetic energy and turbulent dissipation. Since the flow is supersonic and compressible, the density-based solver has been activated. The uncontrolled jet is simulated using the axisymmetric computational region surrounding the jet centreline. However, the near-field region of the cross-wire, located at the nozzle exit, captures the flow physics, including vortex dynamics, while the mixing ability of the controlled jet is assessed over the entire computational domain. The realizable k-ε turbulence model has been employed to capture the turbulence, suggested by many researchers in the past [28, 32-34]. The structured mesh was devel-

oped with local refinement in the wall and flow-separation regions. The final mesh consisted of approximately 6.36 lakh cells. A combination of grid sets (coarse, medium, and fine) was evaluated. Important output parameters, such as velocity profiles, exhibited nearly 2% variation between the medium and fine grids, indicating mesh independence. The density-based solver was used. Pressure-velocity coupling was handled using the SIMPLE scheme, with second-order discretization applied to the pressure, momentum, and turbulence equations. The convergence criteria of 10^{-5} has been set in-order to attain a substantial level of accuracy for the solutions. Figure. 9 presents the residual plots, which demonstrate the convergence and stability of the numerical simulation. The pressure inlet boundary condition is specified, and the pressure values are varied according to the NPR requirements. The outlet was at atmospheric pressure. Walls were treated as no-slip boundaries, and symmetry conditions were applied as needed.

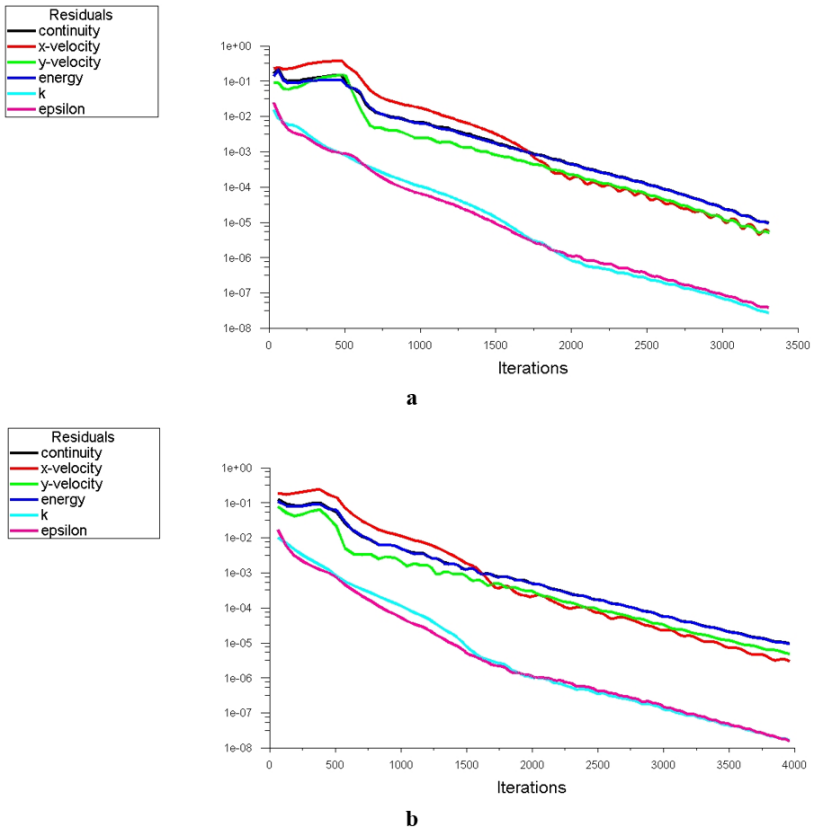

Figure 9. Residuals plot to present the convergence and stability of the numerical simulation: (a) overexpanded jet and (b) under expanded jet

3.5. Computational validation

The established experimental result of Shantanu and Radhakrishnan [20] is compared with the current computational study, presented in Figure 10. The results show the non-dimensional variation of the Pitot pressure as a function of the non-dimensional downstream distance of the jet. At NPR 5, the number of shock cells for this flow is almost identical in both cases. The slight phase discrepancy between numerical and experimental data is due to the perturbation in the outgoing flow from the pitot probe. The presence of the pitot probe at the nozzle exit directly causes the bow shock to occur upstream of it. If an external obstruction exists within the flow regime, the supersonic flows respond to it immediately. The computers demonstrate their ability to create ideal testing conditions. The total pressure downstream of the nozzle can be calculated without substantially altering the normal flow pattern. As a result, there is some variation between the findings obtained experimentally and those computed using governing equations and applied boundary conditions. Figure 10 shows that this aberration is evident along the jet centreline as a small phase difference on the order of 0.5D. Both the experimental observations and the numerical results demonstrate similar flow features.

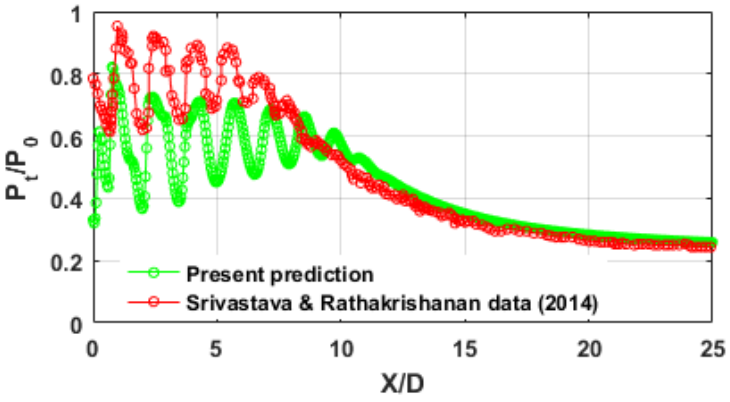

Figure 10. Validation of the current study using Srivastava and Rathakrishana's experimental work [20]

4. Results and discussion

The distance measured axially from the nozzle exit where the centreline velocity of the jet remains supersonic is referred to as the jet's core length in scholarly works [29, 35, 36]. The jet core in the case of a supersonic jet, also known as the supersonic core, has a sinusoidal profile and a continuous series of expansion and compression waves, as shown in Figure. 10, Figure. 11, and Figure. 14. Hence, the supersonic core is the wave-dominated region downstream of the nozzle exit. The diminishing of wave-dominated curves and the steep decay of centreline pressure or velocity indicate the effective transport of ambient fluid mass toward the jet centerline, leading to a continuous decrease in jet centreline velocity due to momentum transport. The jet's mixing ability and supersonic core length are inversely correlated. This evidence shows that a shorter core is associated with better mixing than a longer core. In the jet literature, the terms "extent of jet mixing" and "rate of jet mixing" denote distinct concepts. The jet core length measurement indicates the extent to which the jet has mixed with the surrounding air. The distinctive decay zone that tracks the length of the jet core provides a more comprehensive understanding of the rate of jet mixing. The self-similar zone, which strictly falls within the fluid-mechanics regime and is not affected by gas-dynamic relations, lies beyond the typical decay zone. The centreline velocity decay (or centreline pressure decay) (Figures. 11 and 14) and the rate of jet spread (Figs. 12, 13, 15, and 16) were adopted to evaluate performance.

4.1. Effect of NPR on the jet mixing

Figure 11(a) displays the overall pressure variation with respect to the jet axis. Due to the extremely unfavourable pressure gradient at the nozzle exit, an overexpansion of 36.5% was reported at NPR 4. Due to a high adverse pressure gradient at the nozzle exit, a strong oblique shock occurs at the nozzle edge to stabilize the flow. The jet core length is approximately 4.5D downstream of the nozzle exit for both the jet with a tab and the jet without a tab. The jet without a tab has four shock cells, while the jet with one has three.

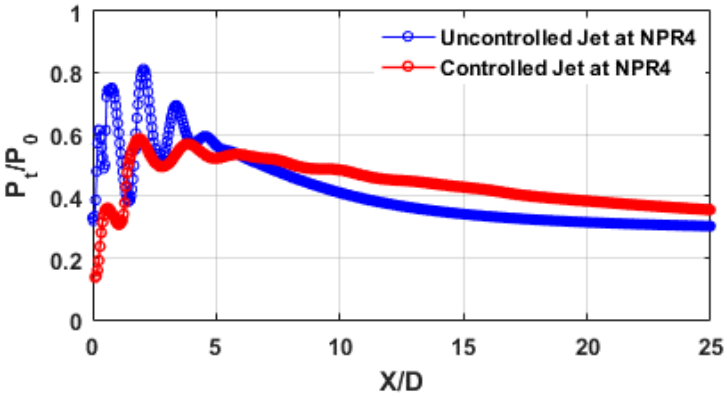

Figure 11(a). CPD at NPR 4

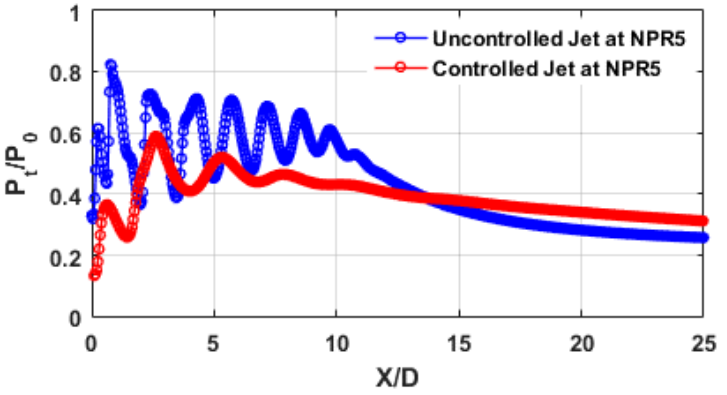

Figure 11(b). CPD at NPR 5

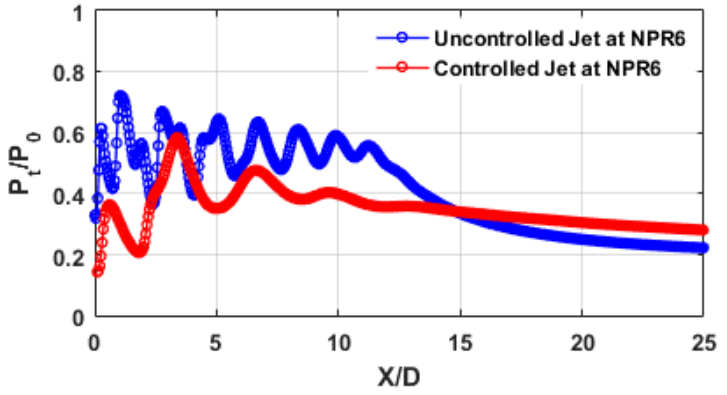

Figure 11(c). CPD at NPR 6

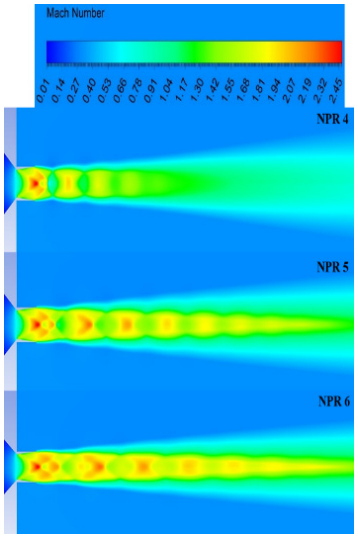

Figure 12. Mach number visualization of an uncontrolled, overexpanded jet at NPR 4, 5, and 6

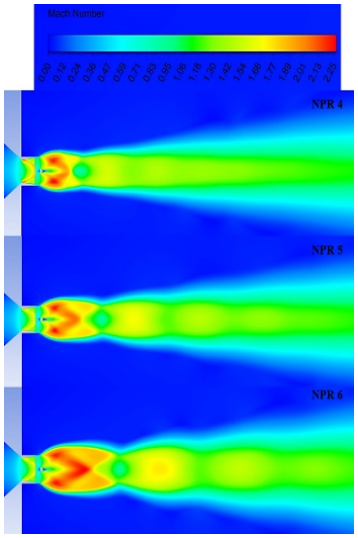

Figure 13. Mach number visualization of controlled, overexpanded jet at NPR 4, 5 and 6

This image effectively illustrates the increased rate of jet mixing, as shown by the distinctive decay zone in each case. Figure 11(b) depicts the state of the jets studied at NPR 5 and shows that a cross-wire can shed vortices that improve jet mixing and reduce core length by 27%. At NPR 5, the total number of shock cells decreased from 8 to 4, as indicated by the centreline pressure-decay measurements. Vortex mechanics play a major role in determining the extent of jet mixing.

Compared with the uncontrolled jet, the number of shock cells at NPR 6 does not change substantially, but the length of each shock-cell structure increases (Figure 11(c)). At the nozzle exit, an unfavourable pressure gradient of approximately 5% is present under NPR 6 at Mach 1.86, resulting in a 21% reduction in core length.

At NPR 7, a marginally favourable pressure gradient is observed, which causes the core length to decrease by around 18%, as depicted in Figure 14(a). The favourable pressure gradient at the nozzle exit forces the outgoing flow to accelerate and veer away from the mean flow direction. Waves alter the characteristics and directions of a typical supersonic flow. The expansion fans created at the nozzle lip by the favourable pressure gradient accelerate the flow. When the NPR is raised from 7 to 8, the favourable pressure rises and the controlled jets' mixing capacity is enhanced (Figure 14(b)).

The reduction in core length at NPR 8 is approximately 28%. A 37% decrease in core length is reported at NPR 9, along with a further increase in the favourable pressure gradient, Figure 14(c). As the NPR rises, the mixing ability of the cross-wire-controlled jet increases beyond the correct expansion condition and decreases near the correct expansion condition. This response may be influenced by the rate at which vortices generated in shear layers near the jet boundary approach the jet centreline. The jet becomes increasingly under expanded at high nozzle pressure ratios, resulting in a pronounced increase in shock-cell strength and in the pressure gradient at the nozzle exit. At NPR 9, the stronger interaction between the shock cells and the surrounding shear layers stimulates Kelvin-Helmholtz instabilities, which in turn enhance the formation of large-scale vortices. The jet core becomes more vortical because increased axial momentum transfer enhances transverse fluid mixing and jet-core entrainment. The same mechanism of shock–vortex interaction and increased shear-layer growth in under expanded jets has been documented (Zaman 1999 [1]; Tam & Tanna 1982 [3]; Panda & Seasholtz 1999 [4]). In contrast, under NPR 8 conditions, the jet expansion is weaker, resulting in less intense shocks and less vigorous shear-layer instabilities. Consequently, vortex activity is weaker, and mixing enhancement is reduced.

A positive pressure gradient created by a rise in NPR accelerates flow, and momentum is transferred at the jet boundary. As transverse momentum increases, vortices formed at the jet boundary approach the jet centreline more rapidly. Additionally, as the flow accelerates, the flow velocity and Mach number increase concomitantly with a favourable pressure gradient. The vortices created by the cross-wire become stronger and larger, and are shed more frequently due to the increased flow velocity. Consequently, as NPR rises, the tab's mixing capacity increases.

4.2. Qualitative visualization of shocks present in the jet

Figures 12, 13, 15, and 16 display qualitative visualizations of controlled and uncontrolled jets. Figures 12 and 15 demonstrate how the number and strength of shock cells increase as NPR rises. Nearly the same number of shock cells is visible at higher NPR values (NPR 7 to NPR 9), but the shock cells are stronger than those found at earlier jet NPRs. Because of a favourable pressure gradient, the Mach disk nucleates at greater under expansion (NPR8 and NPR9). The insertion of a limiting tab at the nozzle outlet results in nearly the

same number of shock cells as observed in the controlled jet's Mach contours (Figures 13 and 16). However, the shock strength increases noticeably as the NPR increases.

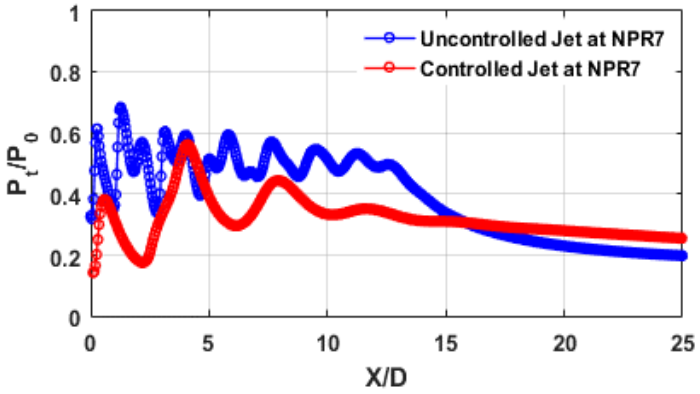

Figure 14(a). CPD at NPR 7

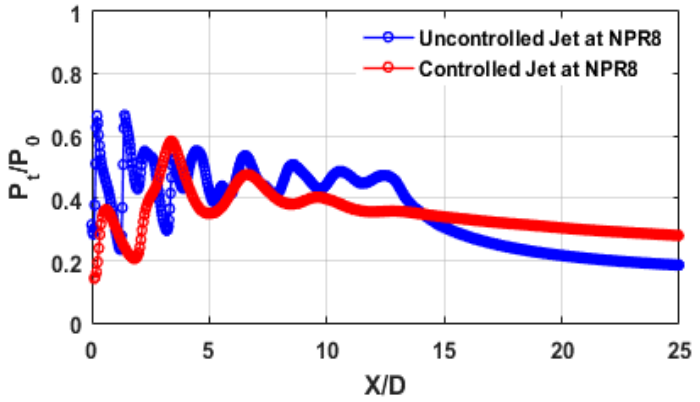

Figure 14(b). CPD at NPR 8

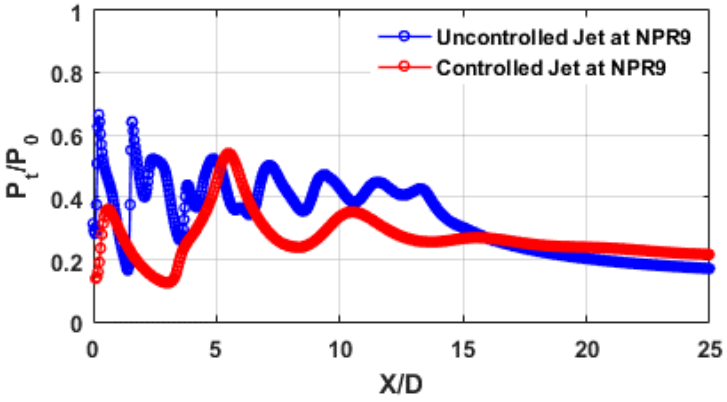

Figure 14(c). CPD at NPR 9

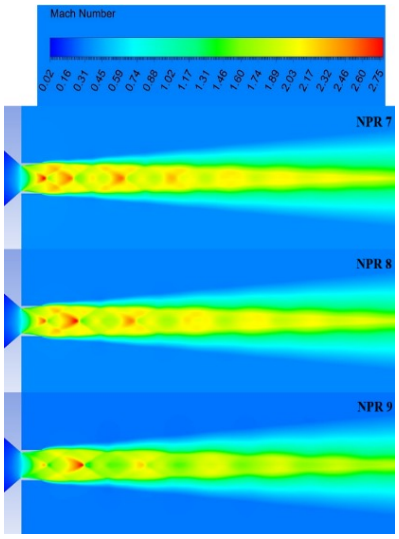

Figure 15. Mach number visualization of an uncontrolled, underexpanded jet at NPR 7, 8, and 9

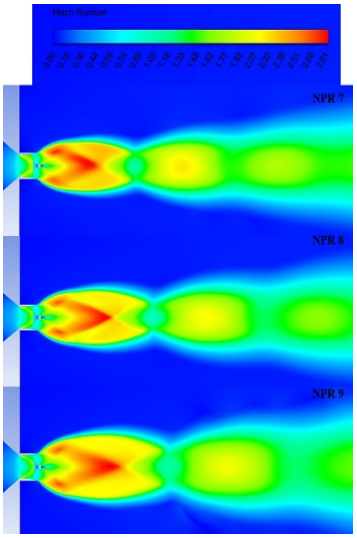

Figure 16. Mach number visualization of an uncontrolled, underexpanded jet at NPR 7, 8, and 9

Only The first shock cells of each NPR (NPR 4 to NPR 9) are stronger, as demonstrated by the Mach contours of the controlled jet (Figures 13 and 16). Additionally, each shock cell in the controlled jets expands markedly with increasing NPR. Mach contours and the centerline pressure-decay plot indicate that the mixing ability of the cross-wire-controlled jet increases with increasing favourable pressure gradient.

At nearly correct expansion conditions, the jet core length is observed to be minimal. Although the length of each shock cell increases as the NPR rises, the total number of shock cells remains constant. At the maximum NPR in the current study, Mach disk

nucleation occurs in the Mach 1.86 jet. The core lengths of both uncontrolled and controlled jets, together with the number of shock cells at NPR, are summarized in Table 3.

Table 3. Quantitative reduction in jet core length and shock cells using passive control technique

Types of Jet	Uncontrolled Jet		Controlled Jet	
NPR	Core length	No. of shock cells	Core length	No. of shock cells
NPR 4	4.75D	4	4.50D	3
NPR 5	11.00D	8	8.00D	4
NPR 6	11.50D	7	9.50D	4
NPR 7	13.00D	7	11.00D	3
NPR 8	12.50D	6	9.75D	3
NPR 9	14.00D	6	10.25D	3

4.3. Comparative analysis with literature

The present simulations are consistent with supersonic jets studied experimentally and numerically. Earlier measurements and analyses indicate that with stronger under expansion (higher NPR) the shocks and shear-layer interactions become more intense, leading to increased shear-layer instability that enhances jet core contraction and shortening (Zaman 1999 [1]; Tam & Tanna 1982 [3]; Panda & Seasholtz 1999 [4]). The benchmark data of free jets by Hussein et al. 1994 [37] and Panchapakesan & Lumley 1993 [38] demonstrate the canonical decay of centerline and jet spreading that is also present in the current results.

On that basis, the current controlled-jet cases indicate relative reductions of ~21–27% at NPR 5–6 and ~37% at NPR 9 relative to the baseline uncontrolled-jet core lengths. Even though, due to variation in Reynolds number, and control mechanism, the absolute reduction percentages may differ among investigations, the direction and relative magnitude of the changes are in line to the experimental documentation of passive control systems (tabs, wires, chevrons) that augment shear-layer growth and entrainment (Zaman, 1999 [1]); Rajaratnam, 1976 [2]). The NPR 9 reduction still supports experimental results stating that under expanded jets exhibit stronger shock–vortex interactions which enhance vortex roll-up and mixing (Panda & Seasholtz, 1999 [4]).

The larger reductions noted above may be due to (i) the cross-wire architecture and the geometry of the configuration, which directly perturb the shear layer at the nozzle exit; (ii) the 2-D model approximation, which tends to amplify planar vortex structures; and (iii) the turbulence closure used (realizable k–ε), which differs from the LES/experimental statistics used. Taken together, the comparison shows that these findings are consistent with current literature trends and that a simple cross-wire can yield substantial passive mixing enhancement across a wide range of NPRs.

5. Conclusion

The study investigates enhancement of mixing in a Mach 1.86 supersonic jet through a passive control technique. A rectangular cross-wire with a 5% area blockage ratio is installed at the nozzle exit to achieve passive control. The uncontrolled jet is compared with the controlled jet. The results show that the decrease in core length is influenced by the pressure gradient at the nozzle exit. An under expanded state with a favourable pressure gradient exists for NPR > 6, whereas an overexpanded state with an unfavourable pressure gradient exists for NPR ≤ 6. The core length reduction increases with NPR after NPR 6 and decreases with NPR up to NPR 6. The study also found that jet mixing occurs more rapidly at higher levels of overexpansion. Comparable patterns were observed at the elevated level of under expansion, with a jet-core reduction of approximately 37% at NPR9. Although the study is based on two-dimensional CFD simulations, it demonstrates the novel use of a plain rectangular cross-wire for supersonic jet control, which is passive and cost-effective. These passive changes have practical applications in systems where improved jet mixing is necessary, such as noise reduction and improvements in combustion and propulsion system efficiency.

6. Future work

Although the effectiveness of a rectangular cross-wire in promoting supersonic jet mixing the current study demonstrates, some questions remain that require further analysis. Further studies are required using three-dimensional simulations and advanced turbulence modelling techniques such as LES or hybrid RANS–LES methods, which are able to account for the transient vortex dynamics and shock–turbulence interaction. Applications include jet noise suppression in aerospace propulsion and enhanced fuel–air mixing in supersonic combustors, thereby highlighting the practical relevance of such simplicity.

Disclosure of interest

No potential competing interests were reported by the authors.

Funding

No funding was received.

Copyright and permission statement

All figures included in this manuscript are original works created by the authors. No third-party copyrighted material has been reproduced or adapted.

Nomenclature

T	Absolute temperature (K)
k	Coefficient of thermal conductivity (W/m.K)
e	Internal energy per unit mass (J/kg)
S	Mean strain rate (s^{-1})
p	Pressure (N/m^2)
q	Rate of heat generation per unit volume (W/m^3)
S_{ij}	Strain tensor
t	Time (s)
P_k	Generations of turbulent kinetic energy due to buoyancy (m^2/s^3)
P_b	Generations of turbulent kinetic energy due to mean velocity gradient (m^2/s^3)
f_x	X-component body force per unit mass (m/s^2)
f_y	Y-component body force per unit mass (m/s^2)
u	X-component of the velocity(m/s)
v	Y-component of the velocity(m/s)
S_k	User-defined source terms for turbulent kinetic energy (m^2/s^3)
S_ϵ	User-defined source terms for turbulent dissipation (m^2/s^3)
$\vec{V}$	Velocity vector (m/s)

Greek symbols

Ω_{ij}	Average rate-of-rotation tensor
μ	Coefficient of dynamic viscosity
μ_t	Coefficient of eddy viscosity
σ_ε	Prandtl number associate with turbulent dissipation
σ_k	Prandtl number associate with turbulent kinetic energy
ρ	Mass density of the fluid (kg/m^3)
τ_{xx}	Normal stress (N/m^2)
τ_{xy}	Shear stress (N/m^2)

References

[1] Zaman, K.B.M.Q., 1999. Spreading characteristics of compressible jets from nozzles of various geometries. Journal of Fluid mechanics, 383, pp.197-228.

[2] Rajaratnam, N., 1976. Turbulent jets (Vol. 5).Elsevier.

[3] Tam, C.K. and Tanna, H.K., 1982. Shock associated noise of supersonic jets from convergent-divergent nozzles. Journal of Sound and Vibration, 81(3),pp.337-358.

[4] Panda, J. and Seasholtz, R.G., 1999. Measurement of shock structure and shock–vortex interaction in under expanded jets using Rayleigh scattering. Physics of Fluids, 11(12),pp.3761-3777.

[5] Bradbury, L.J.S. and Khadem, A.H., 1975. The distortion of a jet by tabs. Journal of fluid mechanics, 70(4),pp.801-813.

[6] Zaman, B., Reeder, M. and Samimi, M., 1992, January. Supersonic jet mixing enhancement by delta-tabs. In 28th Joint Propulsion Conference and Exhibit (p. 3548).

[7] Zaman, K.B.M.Q., 1993, July. Streamwise vorticity generation and mixing enhancement in free jets by 'delta-tabs'. In 3rd shear flow conference (p. 3253).

[8] Ahuja, K. and Brown, W., 1989, March. Shear flow control by mechanical tabs. In 2nd Shear flow conference (p. 994).

[9] Zaman, K.B.M.Q., Reeder, M.F. and Samimi, M., 1994. Control of an axisymmetric jet using vortex generators. Physics of Fluids, 6(2),pp.778-793.

[10] Zaman, K.B.M.Q., Reeder, M.F. and Samimi, M., 1993. Effect of Tab Geometry on the Flow and Noise Field of an Axisymmetric Jet. AIAA Journal, 31(4), pp. 609–619.

[11] Singh, N.K. and Radhakrishnan, E., 2002. Sonic jet control with tabs. International Journal of Turbo and Jet Engines, 19(1-2),pp.107-118.

[12] Srivastava, S., and Radhakrishnan, E., 2014. Performance of Corrugated Limiting Tab in Presence of Sharp Corner, International Review of Aerospace Engineering, 7(1), pp. 1– 7.

[13] Shantanu Srivastava and Mrinal Kaushik, Supersonic Square Jet Mixing in Presence of Cross-Wire at Nozzle Exit, American Journal of Fluid Dynamics, 5(3A), 2015: 19 – 23.

[14] Balaji, K., Gore, M.R. and Kandal, S.V., 2022, August. Numerical and experimental study of vortex generator. In Biennial International Conference on Future Learning Aspects of Mechanical Engineering (pp. 249-260).Singapore: Springer Nature Singapore.

[15] Ranganathan, M., Mohana Saravanan, Akhil, Shankar, M. and Munisamy, S., 2023, June. Validation of experimental studies of subsonic jets controlled by air tabs through simulation studies. In 5th International Conference on innovative design, analysis & development practices in aerospace & automotive engineering: I-DAD'22 (Vol. 2766, No. 1, p. 020025). AIP Publishing LLC.

[16] Nayak, D., Jamael, S., CK, A., Ramesh Bhai, P.A. and Saranya, S., 2025. Investigation of the Combined Injection and Vortex Generator Method for Aerofoil Performance Enhancement. International Journal of Aeronautical and Space Sciences, pp.1-10.

[17] Raj, R.A., Balguri, P.K., Anand, M.D., Akhil, C.K., Darwins, A.K. and Belchada, R., 2024. Fabrication and flow simulation of a choked flow converging nozzle. International Journal of Vehicle Structures & Systems, 16(3),pp.356-359.

[18] Akhil, C.K., Balaji, K., Baranwal, S., Sohany, F.A., Gupta, S., Sorowar, S.B. and Tejnarayan, S.A., 2025. Numerical analysis of scramjet combustion chamber under varied strut configuration. Aerospace Systems, 8(3),pp.645-658.

[19] Manikanta, T.V.S. and Sridhar, B.T.N., 2024. Effect of wall length on an interacting supersonic rectangular jet. Aircraft Engineering and Aerospace Technology, 96(5),pp.736-746.

[20] Illyas, S.M., Bapu, B.R. and Manokar, A.M., 2021. Experimental and computational study of heat transfer and flow structure of slotted impinging jet. Journal of Thermal Engineering, 10(5),pp.1275-1291.

[21] Thakare, H.R., 2025. Computational investigation and exergy analysis of swirling flow in vortex tube. Journal of Thermal Engineering, 11(4),pp.1176-1192.

[22] Launder, B.E. and Spalding, D.B., 1974. The numerical computation of turbulent flows. Computer Methods in Applied Mechanics and Engineering, 3(2), pp. 269 – 289.

[23] Dash, S.M., Kenzakowski, D.C., Seiner, J.M. and Bhat, T.R.S., 1993. Recent advances in jet flowfield simulation: Part I-Steady flows. AIAA paper, pp.93-4390.

[24] Thies, A.T. and Tam, C.K., 1996. Computation of turbulent axisymmetric and nonaxisymmetric jet flows using the K-epsilon model. AIAA journal, 34(2),pp.309-316.

[25] Evgenevna, I.E., Evgenevna, I.T. and Viktorovich, B.P., 2014. Analysis of the application of turbulence models in the calculation of supersonic gas jet. American Journal of Applied Sciences, 11(11),pp.1914-1920.

[26] Kumar, B., Verma, S.K. and Srivastava, S., 2024. Mixing enhancement with minimal thrust loss for the Mach 1.76 jet issuing from different beveled collar nozzles. Proceedings of the Institution of Mechanical Engineers, Part E: Journal of Process Mechanical Engineering, p.09544089241287091.

[27] Kumar, B., Verma, S.K. and Srivastava, S., 2021. Effect of collar and bevel angle in mixing enhancement of Mach 1.76 jet exiting from a convergent-divergent nozzle. Applied Engineering Letters: Journal of Engineering and Applied Sciences, 6(1),pp.1-10.

[28] Kumar, B. and Srivastava, S., 2019, July. Modelling 2-D supersonic jet from a convergent-divergent nozzle using k-ε realizable turbulence model. In Journal of Physics: Conference Series (Vol. 1240, No. 1, p. 012019).IOP Publishing.

[29] Rathakrishan, E., 2010. Applied Gas Dynamics. Jhon Wiley & Sons (Asia) Pvt Ltd, Singapore.

[30] Anderson, J.D. and Wendt, J., 1995. Computational fluid dynamics (Vol. 206, p. 332). New York: McGraw-hill.

[31] Wilcox, D.C., 1998. Turbulence modeling for CFD (Vol. 2, pp. 103-217).La Canada, CA: DCW industries.

[32] Lohia, D.K., Kumar, B., Srivastava, S. and Paliwal, H.K., 2018. Numerical simulation of supersonic overexpanded jet from 2-D convergent-divergent nozzle. International Journal of Integrated Engineering, 10(8).

[33] Khavaran, A., Krejsa, E.A. and Kim, C.M., 1994. Computation of supersonic jet mixing noise for an axisymmetric convergent-divergent nozzle. Journal of Aircraft, 31(3),pp.603-609.

[34] Bartosiewicz, Y., Aidoun, Z., Desevaux, P. and Mercadier, Y., 2003, September. CFD-experiments integration in the evaluation of six turbulence models for supersonic ejectors modeling. In Proceedings of Integrating CFD and Experiments Conference, Glasgow, UK.

[35] Kumar, B., Verma, S.K. and Srivastava, S., 2023. Numerical investigation of mixing performance for controlled supersonic jet. Proceedings of the Institution of Mechanical Engineers, Part G: Journal of Aerospace Engineering, 237(11),pp.2602-2616.

[36] Kumar, B., Verma, S.K. and Srivastava, S., 2021. Mixing Characteristics of Supersonic Jet from Bevelled Nozzles. International Journal of Heat & Technology, 39(2).

[37] Hussein, H.J., Capp, S.P. and George, W.K., 1994. Velocity measurements in a high-Reynolds-number, momentum-conserving, axisymmetric, turbulent jet. Journal of Fluid Mechanics, 258, pp.31-75.

[38] Panchapakesan, N.R. and Lumley, J.L., 1993. Turbulence measurements in axisymmetric jets of air and helium. Part 1. Air jet. Journal of Fluid Mechanics, 246, pp.197-223.